Coffill and Lee *et al.* Supplemental Information

Molecular dynamics

Initial structures for molecular dynamics (MD) simulations were taken from the Protein Data Bank (PDB). Human p53 transactivation domain peptide (residues 17-29) and nutlin-3a were extracted from the PDB structures 1YCR (Kussie et al. 1996) and 4J3E (Vu et al. 2013) respectively and modeled onto the human $HDM2^{Nterm}$ structure (residues 17-112) taken from the PDB structure 3JZR (Phan et al. 2010). Using PyMOL (DeLano 2002), the human p53 peptide was extended by one residue at its N-terminus and then capped by acetyl and amide groups, while $HDM2^{Nterm}$ was capped at its N- and C-termini by acetyl and N-methyl groups respectively. Complexes of $HDM2^{Nterm}$ with lamprey p53, lamprey p53 G22L mutant and human p53 triple alanine mutant (F19A, W23A, L26A) peptides were generated by mutating the human p53 peptide to the appropriate sequence. The mutations were performed by keeping the peptide backbone fixed and using the tleap module of AMBER 12 (Case et al. 2012) to add the side chains of the mutated residues. Residue protonation states were determined by PDB 2PQR (Dolinsky et al. 2004). The LEaP program in the AMBER 12 package was then used to solvate each system with TIP3P (Jorgensen et al. 1983) water molecules in a periodic truncated octahedron box, such that its walls were at least 10 Å (12 Å and 15 Å for the unbound peptides and for nutlin-3a, respectively) away from the $HDM2^{Nterm}$ complex and for neutralization of charges with either sodium or chloride ions.

Three independent explicit-solvent MD simulations were carried out on each of the complexes of $HDM2^{Nterm}$ with human p53, human p53 triple alanine mutant, lamprey p53, lamprey p53 G22L mutant and nutlin-3a, as well as the unbound forms of $HDM2^{Nterm}$, p53 peptides and nutlin-3a. Energy minimizations and MD simulations were carried out by the

PMEMD module of AMBER 12, using the ff99SB force field (Hornak et al. 2006) for the protein and peptides and the generalized AMBER force field (Wang et al. 2004) for nutlin-3a. All bonds involving hydrogen atoms were constrained by the SHAKE algorithm (Ryckaert et al. 1977), allowing for a time step of 2 fs. Nonbonded interactions were truncated at 9 Å while electrostatic interactions were treated by the particle mesh Ewald method (Darden et al. 1993). Energy minimization was carried out using the steepest descent algorithm for 500 steps, followed by the conjugate gradient algorithm for another 500 steps. Each system was then heated gradually to 300 K over 50 ps at constant volume before equilibration at a constant pressure (1atm) for another 50 ps. Weak harmonic positional restraints with a force constant of 2.0 kcal mol^{-1} $Å^{-2}$ were imposed on the heavy atoms of the solute during the minimization and these two equilibration steps. Subsequent unrestrained equilibration (2 ns) and production (100 ns) runs were carried out at 300 K and 1 atm. The temperature was maintained using a Langevin thermostat (Izaguirre et al. 2001) with a collision frequency of 2 ps^{-1} while the pressure was maintained by a Berendsen barostat (Berendsen et al. 1984) with a pressure relaxation time of 2 ps.

Binding free energy calculations

Binding free energies for $HDM2^{Nterm}$ complexes were calculated with the molecular mechanics/generalized Born surface area (MM/GBSA) method (Srinivasan et al. 1998). All programs used for MM/GBSA calculations are from AMBER 12. 200 equally-spaced snapshot structures were extracted from the last 10-30 ns of each of the trajectories, depending on when equilibration of the systems occurred (determined from their root mean square deviation plots), and their molecular mechanical energies calculated with the sander module. The polar contribution to the solvation free energy was calculated by the pbsa (Luo et al. 2002) program using the modified generalized Born (GB) model described by Onufriev

et al. (Onufriev et al. 2004) while the nonpolar contribution was estimated from the solvent accessible surface area (SASA) using the molsurf (Connolly 1983) program with $\gamma = 0.0072$ kcal $Å^{-2}$ and β set to zero. The nmode program was used to estimate entropies (Brooks et al. 1995). Due to its computational expense, only 50 equally-spaced snapshots from the equilibrated portion of the trajectories were used for entropic analysis. Replica exchange MD simulations were carried out on the free peptides using standard protocols (Lama et al. 2013).

Binding free energy decomposition

The contribution of each peptide residue to the binding free energy was computed using the free energy decomposition method (Gohlke et al. 2003) on the same 200 snapshot structures used for MM/GBSA analysis. Similar to the MM/GBSA calculations, the molecular mechanical energies and polar contribution to solvation free energy were computed by the sander module and pbsa program using the modified GB model described by Onufriev *et al*. (Onufriev et al. 2004) respectively. The nonpolar contribution to solvation free energy was estimated from the SASA using the ICOSA method (Rarey et al. 1996).

Bio-layer Interferometry (BLI) assay

The affinity of $HDM2^{Nterm}$ binding to the Lamprey peptides was determined using the BLItz (ForteBio, USA) system. The purified $HDM2^{Nterm}$ proteins were buffer exchanged into the kinetics buffer (PBS + 0.05% Tween-20) prior to the experiment. Biotinylated human and lamprey peptides were immobilized at a concentration of 2.5µM on the streptavidin biosensors (ForteBio) which were pre-hydrated in PBS + 5% DMSO for at least 10 minutes. The unbound biotinylated peptides were washed off in the same buffer. The loaded sensors were equilibrated in the kinetics buffer before immersing them into the various titrations of $HDM2^{Nterm}$ (3x serial dilutions from 250µM) over 120 seconds and then immersed into the

kinetics buffer for dissociation. A blank uncoated sensor reference (without biotinylated peptide) was carried out in 250µM HDM2^{Nterm} to ensure no/low binding of HDM2^{Nterm} to the uncoated sensor and a coated sample reference (peptide but without HDM2^{Nterm} protein) was measured as a background binding control. Data analysis was performed using a global fit in the BLItz Pro software to calculate the K_D value.

Amino acid sequence similarity (Table 1)

The amino acid sequence similarities between human and lamprey proteins were determined using pairwise sequence alignment tools (http://www.ebi.ac.uk/Tools/psa/emboss_needle/) (Rice et al. 2000; Li et al. 2015).

Table S1. Computed binding free energies (kcal/mol) of $HDM2^{Nterm}$ complexes.

Ligand	Peptide sequence, if applicable	ΔH_{bind}	$T\Delta S_{bind}$	ΔG_{bind}
nutlin-3a	N.A.	-82.36	-24.08	-58.29
$Hp53^{16-29}$	Ac-QETFSDLWKLLPEN-NH_2	-80.39	-37.21	-43.18
$Hp53^{16-29(AAA)}$	Ac-QETASDLAKLAPEN-NH_2	-79.30	-40.37	-38.92
$Lp53^{12-25}$	Ac-VDDFDRVWQGGVGL-NH_2	-80.61	-40.81	-39.80
$Lp53^{12-25(G22L)}$	Ac-VDDFDRVWQGLVGL-NH_2	-85.63	-37.48	-48.15

Table S2. Experimental determination of binding affinities for peptide and $HDM2^{Nterm}$ complexes

Peptide	Sequence	K_D (μM)[A]	K_D (μM)[B]
$Hp53^{16-29}$	QETFSDLWKLLPEN	2.7 ± 0.5	1.3
$Hp53^{16-29(AAA)}$	QETASDLAKLAPEN	nd	nd
$Lp53^{12-25}$	VDDFDRVWQGGVGL	nd	nd
$Lp53^{12-25(G22L)}$	VDDFDRVWQGLVGL	41 ± 3	33

[A] determined by Fluorescence Anisotropy. Data are averages of at least four replicates ± SEM.

[B] determined by Bio-layer Interferometry (BLI) assay.

nd = not determined due difficulty fitting curve to weak binding data

Table S3. Peptides synthesized for Fluorescence Anisotropy and Bio-layer Interferometry (BLI) assay

Peptide	Sequence	Organism	Reference sequence	Literature reference
FAM-12.1	5(6)-FAM-RFMDYWEGL-NH_2	Human	-	(Bottger et al. 1997)
Hs-p53$^{16-29}$	Ac-QETFSDLWKLLPEN-NH_2		NP_000537.3	
	Biotin-SGSG-QETFSDLWKLLPEN-NH_2			
Hs-p53$^{16-29(AAA)}$	Ac-QETASDLAKLAPEN-NH_2			
	Biotin-SGSG-QETASDLAKLAPEN-NH_2			
Lj-p53$^{12-25}$	Ac-VDDFDRVWQGGVGL-NH_2	Lamprey	KT960978	
	Biotin-SGSG-VDDFDRVWQGGVGL-NH_2			
Lj-p53$^{12-25(G22L)}$	Ac-VDDFDRVWQGLVGL-NH_2			
	Biotin-SGSG-VDDFDRVWQGLVGL-NH_2			

5(6)FAM = mixed isomers 5-(and 6-)carboxyfluoresceine; Ac = acetyl; NH_2 = amide

Table S4. Details of plasmids used in this study

Plasmid	Amino Acids	Tag	Vector	N'/C'	Organism	Reference sequence	Literature reference
Hs-p53	1-393	-	pcDNA3	-	Human	NP_000537.3	
Hs-p53	1-393	3xFLAG 6xHIS	pCI-neo	N'			(Coffill et al. 2012)
Hs-p53Δ	1-355	-	pcDNA3	-			
HDM2	1-491	-	pCMV	-		Q00987	
$HDM2^{Nterm}$	1-125	HA	pcDNA3	C'			
GST-$HDM2^{Nterm}$	1-125 or 6-125	GST-precision	pGEX-6P-1	N'			(Bottger et al. 1997; Brown et al. 2013; Chee et al. 2014)
Hs-RPL11	1-178	FLAG	pcDNA3	N'		NP_000966.2	
Hs-RPL5	1-297	FLAG	pcDNA3	N'		NP_000960.2	
Lj-p53	1-428	3xFLAG 6xHIS	pCI-neo	N'	Lamprey	KT960978	
Lj-p53	1-428	FLAG	pcDNA3	N'			
Lj-p53(G22L)	1-428 (G22L)	FLAG	pcDNA3	N'			
Lj-p53Δ	1-390	FLAG	pcDNA3	N'			
Lj-Mdm2	1-603	HA	pXJ40	N'		KT960981	
Lj-Mdm2(C464A) (human #)	1-603(C576A)	HA	pXJ40	N'			
Lj-Mdm2	1-603	HA	pCMV	C'			
Lj-Mdm2	1-603	HA	pcDNA3	C'			
Lj-$Mdm2^{Nterm}$	1-106	HA	pcDNA3	C'			
Lj-Mdm4	1-280	myc	pCMV	N'		KT960982	

Coffill and Lee *et al.* Supplemental Figure Legends

Figure S1. Alignment of p53
Alignment of p53 protein sequences from lamprey (GenBank accession number KT960978); elephant shark (Eshark) (G9J1L8); zebrafish (P79734); *Xenopus laevis* (frog) (P07193); chicken (P10360); mouse (NP_035770.2) and human (P04637). Alignments were carried out using Clustal Omega (Goujon et al. 2010; Sievers et al. 2011) and Jalview (Waterhouse et al. 2009).

Figure S2. Isoforms of p53
Alignment of p53 isoform protein sequences from human (Hs), zebrafish (Dr) and lamprey (Lj): Hs-p53 (P04637); Hs-Δ40p53 **(**NP_001119590.1); Hs-Δ133p53 (NP_001119587.1); Hs-Δ160p53 (NP_001263626.1); Dr-p53 (P79734); Dr-Δ18p53 (see (Davidson et al. 2010)); Dr-Δ113p53 (see (Marcel et al. 2011)); Lj-p53 (KT960978); Lj-Δ27p53; Lj-Δ30p53; Lj-Δ108p53.

Figure S3. Synteny of *Tp53, Tp63* and *Tp73* genes
Tp53, *Tp63* and *Tp73* gene loci in human, coelacanth and lamprey. Genes that are colored indicate genes that show conserved synteny. The orientation of the pentagons (genes) denotes the direction of transcription and circles represent end of scaffold.

Figure S4. Intron positions of Lj-p53, Lj-p63 and Lj-p73
Alignment of Lj-p53, Lj-p63 and Lj-p73 proteins indicating the positions of introns. The alignment was generated using Clustal Omega. The phase of each intron is indicated by color: yellow (phase 0), green (phase 1), red (phase 2).

Figure S5. Alignment of p63
Alignment of p63 protein sequences from lamprey (GenBank accession number KT960979); elephant shark (Eshark) (G9J1L9); zebrafish (A7YYJ7); *Xenopus tropicalis* (frog) (F6ZGN7); chicken (F1N8Z7); mouse (O88898) and human (Q9H3D4).

Figure S6. Alignment of p73
Alignment of p73 protein sequences from lamprey (GenBank accession number KT960980) elephant shark (Eshark) (G9J1M0); zebrafish (B0S576); *Xenopus tropicalis* (frog) (F6TKT0); chicken (XP_417545.3); mouse (Q9JJP2) and human (O15350).

Figure S7. Gene structure of *Tp63* and *Tp73*
Gene structure and isoforms of *Lj-Tp63* (A) and *Lj-Tp73* (B). Coding exons are designated by open boxes and non-coding exons by shaded boxes. The transcription start site is indicated by an arrow. The sizes of 5' introns are labelled in (A). The longest isoform of *Tp63* has an alternative 5' splice site at the first intron compared with the other two shorter isoforms. The figure is not drawn to scale.

Figure S8. Isoforms of p63
Alignment of p63 isoform protein sequences from human (Hs) and lamprey (Lj): Hs-TAp63α (NP_003713.3); Hs-TAp63β (NP_001108450.1); Hs-TAp63γ (NP_001108451.1); Hs-ΔNp63α (NP_001108452.1); Hs-ΔNp63β (NP_001108453.1); Hs-ΔNp63γ (NP_001108454.1); Lj-p63_A (KT960979); Lj-p63_B and Lj-p63_C.

Figure S9. Alignment of Mdm2
Alignment of Mdm2 protein sequences from lamprey (GenBank accession number KT960981) elephant shark (Eshark) (G9J1M1); zebrafish (Q561Z0); *Xenopus laevis* (frog) (P56273); chicken (F1NGX6); mouse (P23804) and human (Q00987).

Figure S10. Alignment of Mdm RING
Alignment of Mdm2 and Mdm4 protein sequences with HMD2 (Q00987); HDM4 (O15151); Lj-Mdm2 (KT960981) and Lj-Mdm4 (KT960982). Arrows denote the amino acid residues required for either p53 ubiquitination and/or degradation (Fang et al. 2000; Dolezelova et al. 2012).

Figure S11. Alignment of Mdm4
Alignment of Mdm4 protein sequences from lamprey (GenBank accession number KT960982) elephant shark (Eshark) (G9J1M2); zebrafish (Q7ZUW7); *Xenopus tropicalis* (frog) (B5DFR1); chicken (E1C4B0); mouse (O35618) and human (O15151).

Figure S12. Synteny of *Mdm2* and *Mdm4* genes
Mdm2 and *Mdm4* gene loci in human, coelacanth, elephant shark and lamprey. Genes that are colored indicate genes that show conserved synteny. The orientation of the pentagons (genes) denotes the direction of transcription and circles represent end of scaffold.

Figure S13. Averaged binding free energy contributions of peptide residues in the complexes of $HDM2^{Nterm}$ with Hs-$p53^{16-29}$ (blue), Lj-$p53^{12-25}$ (red) and Lj-$p53^{12-25(G22L)}$ mutant (black).

Figure S14. Snapshots of free peptides from Replica exchange molecular dynamics simulations.

Figure S15.
(A) Western blot showing *in vitro* translation (IVT) and immunoprecipitation (IP) of lamprey p53 (top panel) by Lj-Mdm2, which were used as bait. Input levels can be seen in the lower panel. (B) Western blot of Lj-p53 levels following co-transfection with various Lj-Mdm2 expressing constructs. Lanes: (1) Lj-p53; (2) Lj-p53 with MG132; (3) Lj-p53 + HA-Lj-Mdm2; (4) Lj-p53 + HA-Lj-Mdm2 with MG132; (5) Lj-p53 + Lj-Mdm2-HA; (6) Lj-p53 + Lj-Mdm2-HA with MG132; (7) Lj-p53 + Lj-Mdm2-HA + myc-Lj-Mdm4; (8) Lj-p53 + Lj-Mdm2-HA + myc-Lj-Mdm4 with MG132; (9) Lj-p53 9 + myc-Lj-Mdm4; (10) Lj-p53 + myc-Lj-Mdm4 with MG132. Lj-Mdm2 levels can be seen in the upper panel and the loading control can be found in the lower panel.

Figure S16.
(A) A surface presentation (pink) of the human crystal structure of $HDM2^{Nterm}$ (residues 25–109) in complex with Nutlin (B) A surface presentation (green) of a homology model of the p53-binding region of Lj-$Mdm2^{Nterm}$, in complex with Nutlin. Models were generated based on the $HDM2^{Nterm}$ structure (residues 17-112) from the PDB structure 3JZR (Phan et al. 2010).

Supplemental References

Berendsen HJC, Postma JPM, Vangunsteren WF, Dinola A, Haak JR. 1984. Molecular dynamics with coupling to an external bath. *J Chem Phys* **81**: 3684-3690.

Bottger A, Bottger V, Sparks A, Liu WL, Howard SF, Lane DP. 1997. Design of a synthetic Mdm2-binding mini protein that activates the p53 response in vivo. *Curr Biol* **7**: 860-869.

Brooks BR, Janezic D, Karplus M. 1995. Harmonic analysis of large systems. I. Methodology. *J Comput Chem* **16**: 1522-1542.

Brown CJ, Quah ST, Jong J, Goh AM, Chiam PC, Khoo KH, Choong ML, Lee MA, Yurlova L, Zolghadr K et al. 2013. Stapled peptides with improved potency and specificity that activate p53. *ACS Chem Biol* **8**: 506-512.

Case DA, Darden TA, Cheatham TE, Simmerling CL, Wang J, Duke RE, Luo R, Walker RC, Zhang W, Merz KM et al. 2012. AMBER 12. University of California, San Francisco.

Chee SM, Wongsantichon J, Soo Tng Q, Robinson R, Joseph TL, Verma C, Lane DP, Brown CJ, Ghadessy FJ. 2014. Structure of a stapled peptide antagonist bound to nutlin-resistant Mdm2. *PLoS One* **9**: e104914.

Coffill CR, Muller PA, Oh HK, Neo SP, Hogue KA, Cheok CF, Vousden KH, Lane DP, Blackstock WP, Gunaratne J. 2012. Mutant p53 interactome identifies nardilysin as a p53R273H-specific binding partner that promotes invasion. *EMBO Rep* **13**: 638-644.

Connolly ML. 1983. Analytical molecular surface calculation. *J Appl Crystallogr* **16**: 548-558.

Darden T, York D, Pedersen L. 1993. Particle mesh Ewald: an N•log(N) method for Ewald sums in large systems. *J Chem Phys* **98**: 10089-10092.

Davidson WR, Kari C, Ren Q, Daroczi B, Dicker AP, Rodeck U. 2010. Differential regulation of p53 function by the N-terminal DeltaNp53 and Delta113p53 isoforms in zebrafish embryos. *BMC Dev Biol* **10**: 102.

DeLano WL. 2002. The PyMOL Molecular Graphics System. DeLano Scientific, San Carlos, CA, USA.

Dolezelova P, Cetkovska K, Vousden KH, Uldrijan S. 2012. Mutational analysis of Mdm2 C-terminal tail suggests an evolutionarily conserved role of its length in Mdm2 activity toward p53 and indicates structural differences between Mdm2 homodimers and Mdm2/MdmX heterodimers. *Cell Cycle* **11**: 953-962.

Dolinsky TJ, Nielsen JE, McCammon JA, Baker NA. 2004. PDB2PQR: an automated pipeline for the setup of Poisson-Boltzmann electrostatics calculations. *Nucleic Acids Res* **32**: W665-W667.

Fang S, Jensen JP, Ludwig RL, Vousden KH, Weissman AM. 2000. Mdm2 is a RING finger-dependent ubiquitin protein ligase for itself and p53. *J Biol Chem* **275**: 8945-8951.

Gohlke H, Kiel C, Case DA. 2003. Insights into protein-protein binding by binding free energy calculation and free energy decomposition for the Ras-Raf and Ras-RaIGDS complexes. *J Mol Biol* **330**: 891-913.

Goujon M, McWilliam H, Li W, Valentin F, Squizzato S, Paern J, Lopez R. 2010. A new bioinformatics analysis tools framework at EMBL-EBI. *Nucleic Acids Res* **38**: W695-699.

Hornak V, Abel R, Okur A, Strockbine B, Roitberg A, Simmerling C. 2006. Comparison of multiple Amber force fields and development of improved protein backbone parameters. *Proteins: Struct Funct Bioinform* **65**: 712-725.

Izaguirre JA, Catarello DP, Wozniak JM, Skeel RD. 2001. Langevin stabilization of molecular dynamics. *J Chem Phys* **114**: 2090-2098.

Jorgensen WL, Chandrasekhar J, Madura JD, Impey RW, Klein ML. 1983. Comparison of simple potential functions for simulating liquid water. *J Chem Phys* **79**: 926-935.

Kussie PH, Gorina S, Marechal V, Elenbaas B, Moreau J, Levine AJ, Pavletich NP. 1996. Structure of the MDM2 oncoprotein bound to the p53 tumor suppressor transactivation domain. *Science* **274**: 948-953.

Lama D, Quah ST, Verma CS, Lakshminarayanan R, Beuerman RW, Lane DP, Brown CJ. 2013. Rational optimization of conformational effects induced by hydrocarbon staples in peptides and their binding interfaces. *Sci Rep* **3**: 3451.

Li W, Cowley A, Uludag M, Gur T, McWilliam H, Squizzato S, Park YM, Buso N, Lopez R. 2015. The EMBL-EBI bioinformatics web and programmatic tools framework. *Nucleic Acids Res* **43**: W580-584.

Luo R, David L, Gilson MK. 2002. Accelerated Poisson-Boltzmann calculations for static and dynamic systems. *J Comput Chem* **23**: 1244-1253.

Marcel V, Dichtel-Danjoy ML, Sagne C, Hafsi H, Ma D, Ortiz-Cuaran S, Olivier M, Hall J, Mollereau B, Hainaut P et al. 2011. Biological functions of p53 isoforms through evolution: lessons from animal and cellular models. *Cell Death Differ* **18**: 1815-1824.

Onufriev A, Bashford D, Case DA. 2004. Exploring protein native states and large-scale conformational changes with a modified generalized Born model. *Proteins: Struct Funct Bioinform* **55**: 383-394.

Phan J, Li Z, Kasprzak A, Li B, Sebti S, Guida W, Schoenbrunn E, Chen J. 2010. Structure-based design of high affinity peptides inhibiting the interaction of p53 with MDM2 and MDMX. *J Biol Chem* **285**: 2174-2183.

Rarey M, Kramer B, Lengauer T, Klebe G. 1996. A fast flexible docking method using an incremental construction algorithm. *J Mol Biol* **261**: 470-489.

Rice P, Longden I, Bleasby A. 2000. EMBOSS: the European Molecular Biology Open Software Suite. *Trends Genet* **16**: 276-277.

Ryckaert JP, Ciccotti G, Berendsen HJC. 1977. Numerical integration of the Cartesian equations of motion of a system with constraints: molecular dynamics of n-alkanes. *J Comput Phys* **23**: 327-341.

Sievers F, Wilm A, Dineen D, Gibson TJ, Karplus K, Li W, Lopez R, McWilliam H, Remmert M, Soding J et al. 2011. Fast, scalable generation of high-quality protein multiple sequence alignments using Clustal Omega. *Mol Syst Biol* **7**: 539.

Srinivasan J, Cheatham TE, Cieplak P, Kollman PA, Case DA. 1998. Continuum solvent studies of the stability of DNA, RNA, and phosphoramidate−DNA helices. *J Am Chem Soc* **120**: 9401-9409.

Vu B, Wovkulich P, Pizzolato G, Lovey A, Ding Q, Jiang N, Liu J-J, Zhao C, Glenn K, Wen Y et al. 2013. Discovery of RG7112: a small-molecule MDM2 inhibitor in clinical development. *ACS Med Chem Lett* **4**: 466-469.

Wang JM, Wolf RM, Caldwell JW, Kollman PA, Case DA. 2004. Development and testing of a general amber force field. *J Comput Chem* **25**: 1157-1174.

Waterhouse AM, Procter JB, Martin DM, Clamp M, Barton GJ. 2009. Jalview Version 2--a multiple sequence alignment editor and analysis workbench. *Bioinformatics* **25**: 1189-1191.

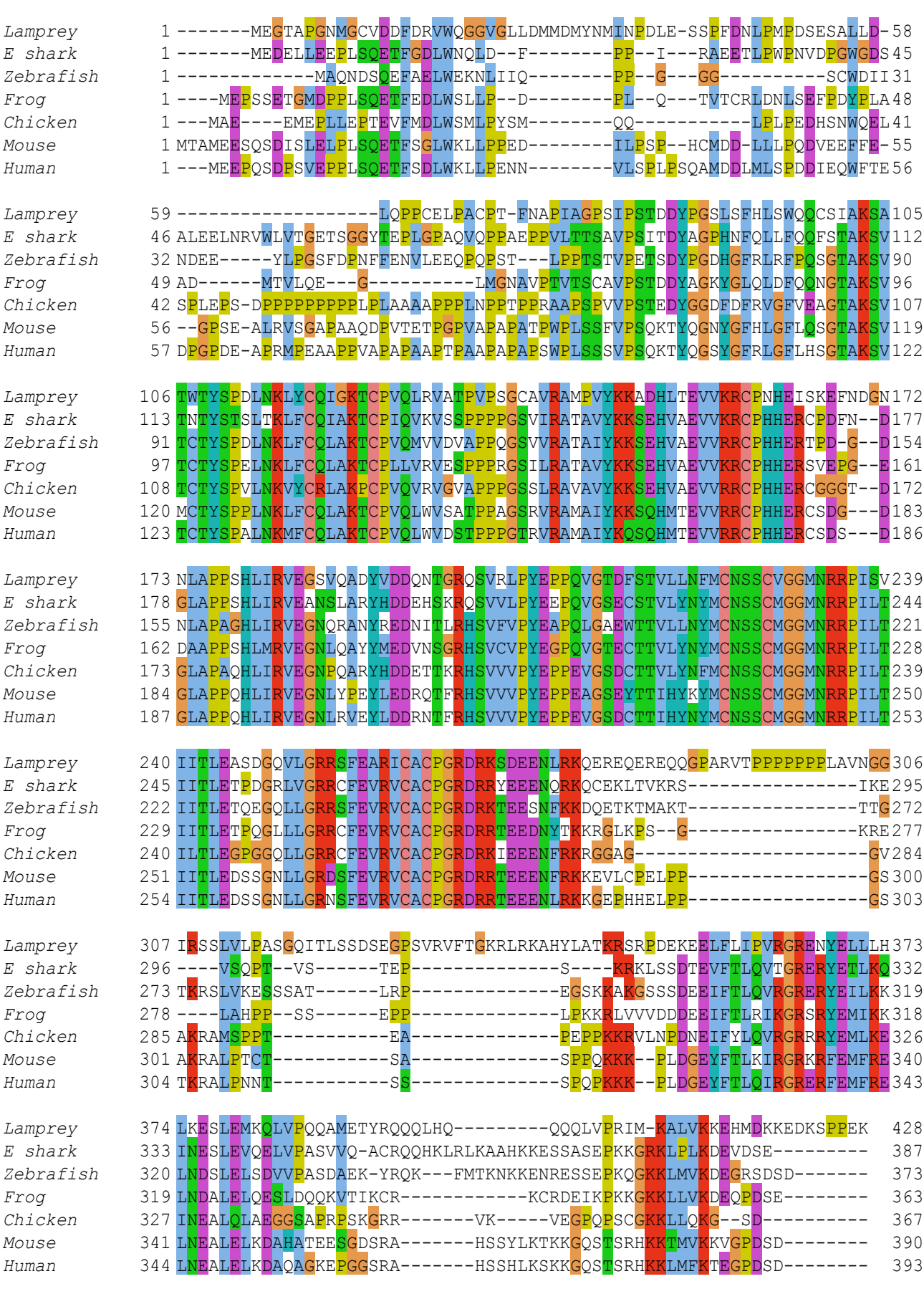

Coffill and Lee *et al.* Fig S1

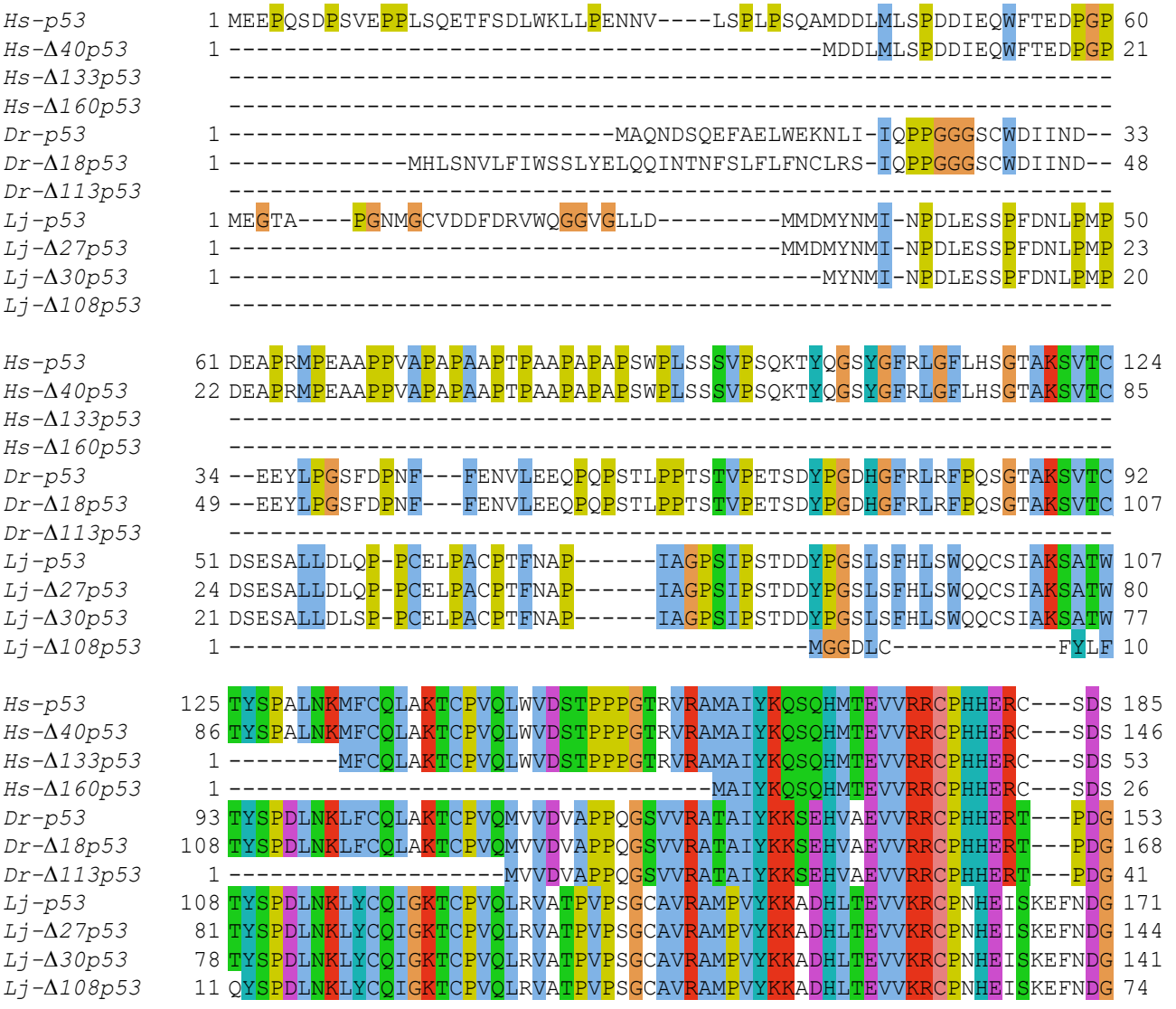

Coffill and Lee *et al.* Fig S2

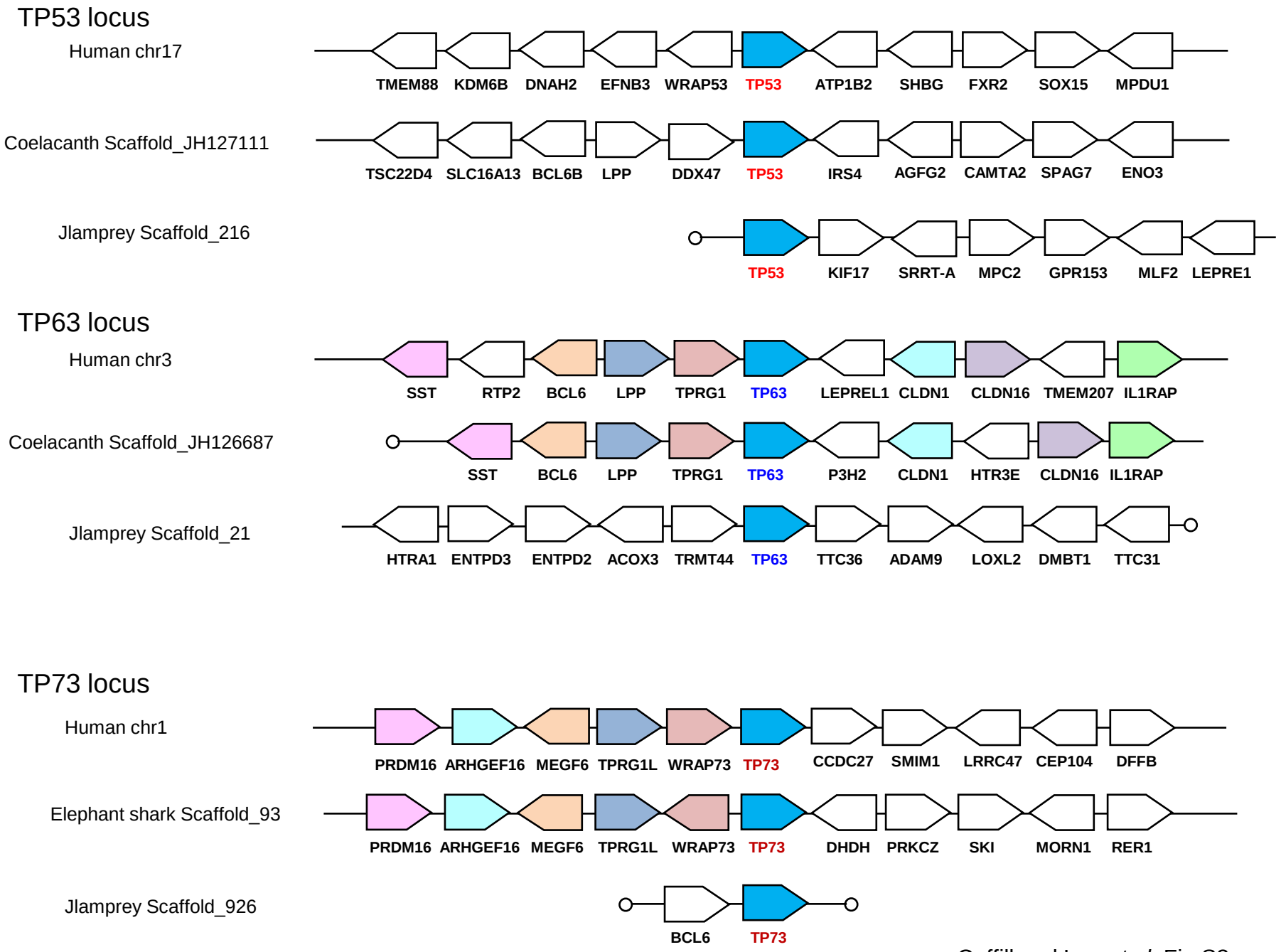

Coffill and Lee *et al.* Fig S3

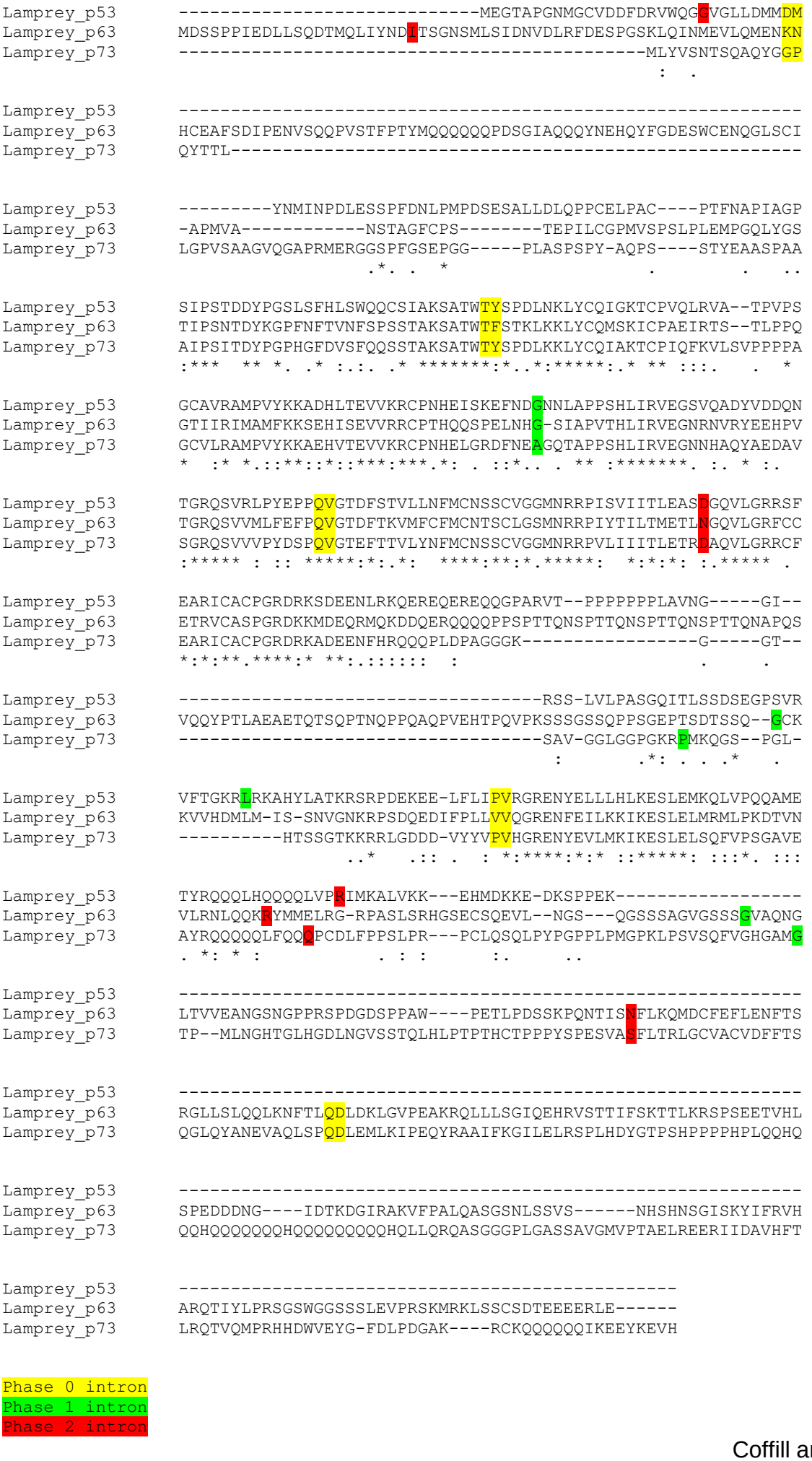

Coffill and Lee *et al.* Fig S4

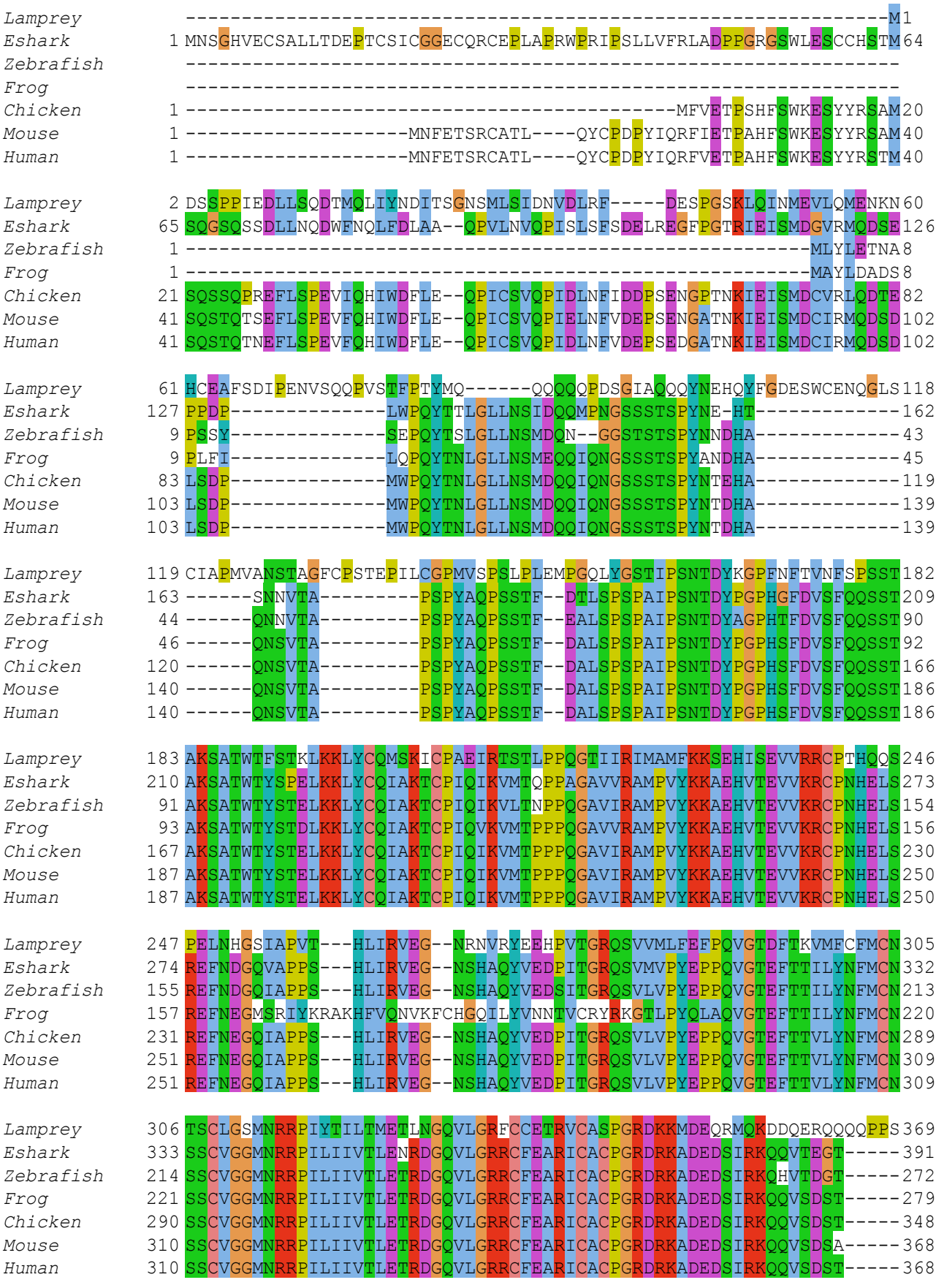

Coffill and Lee *et al.* Fig S5, Panel A

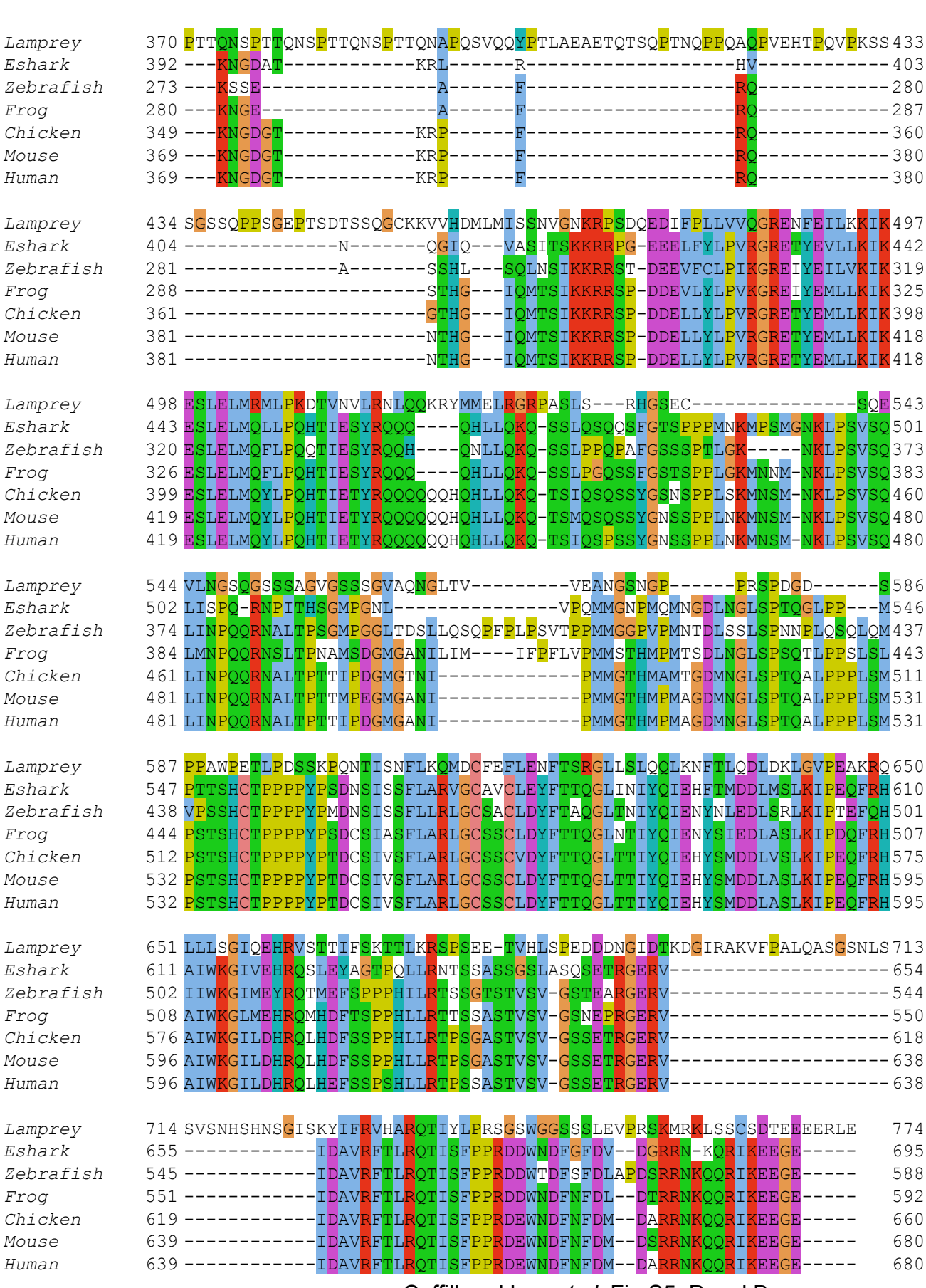

Coffill and Lee *et al.* Fig S5, Panel B

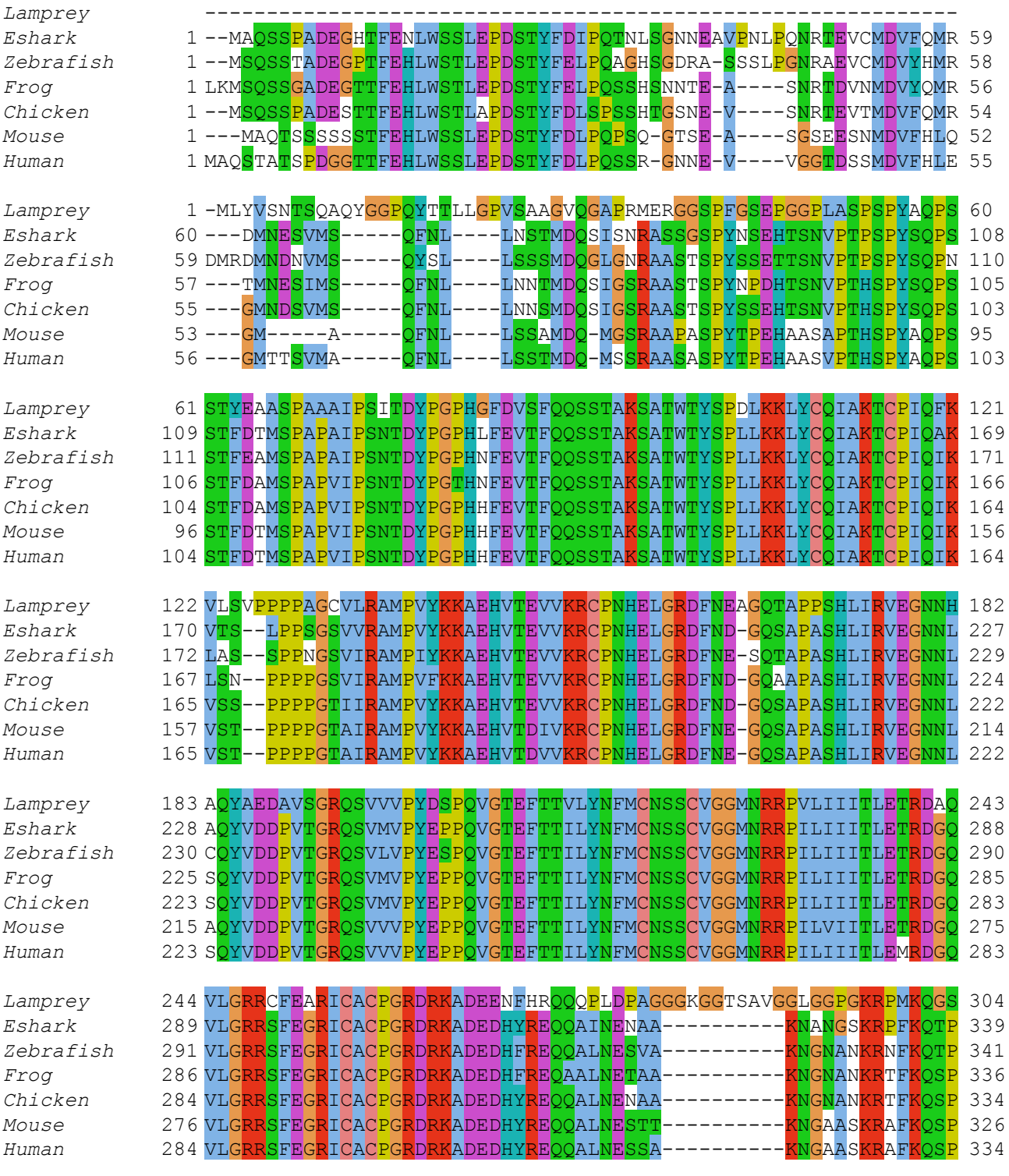

Coffill and Lee *et al.* Fig S6, Panel A

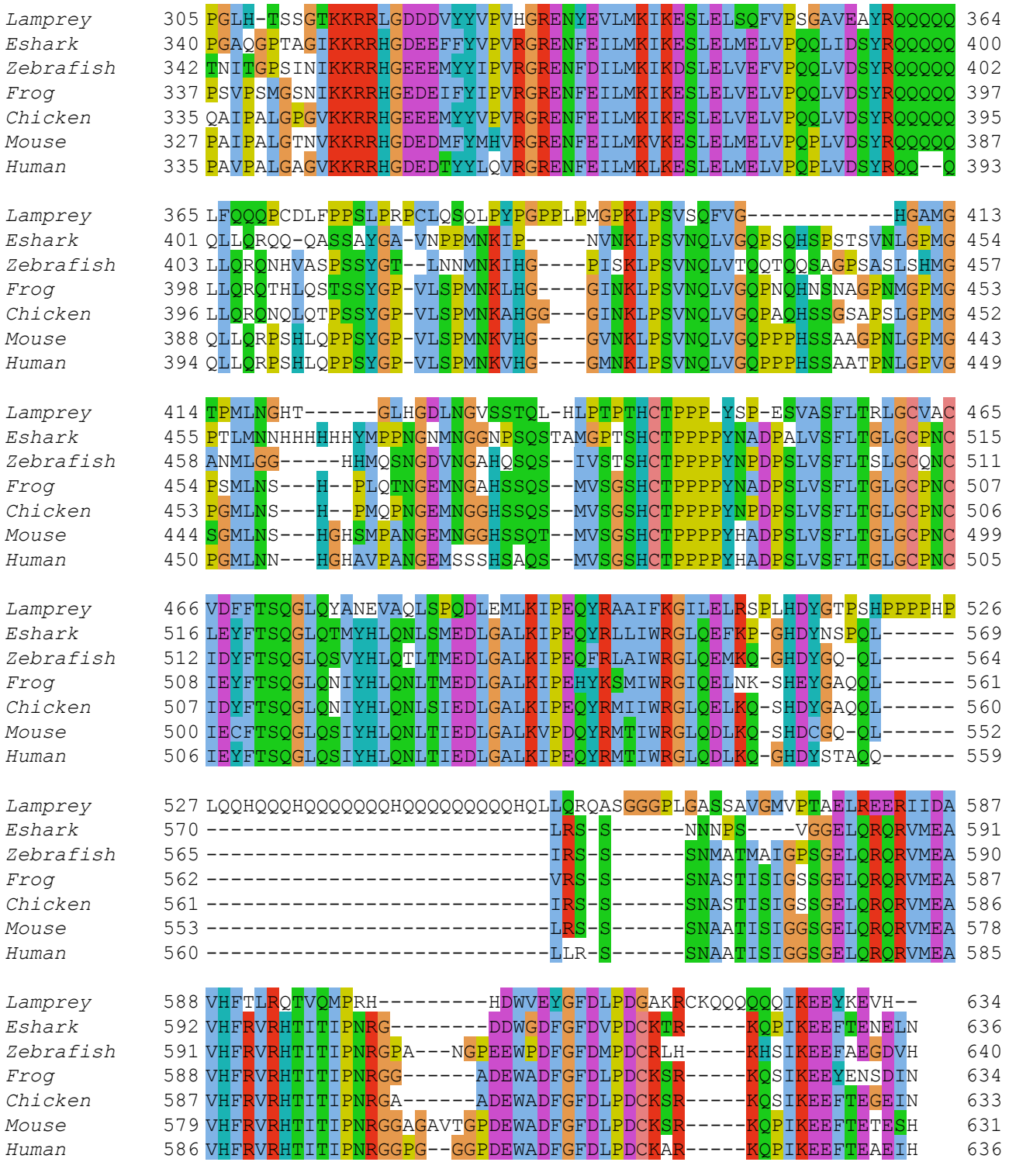

Coffill and Lee *et al.* Fig S6, Panel B

A

Lamprey *Tp63* isoform (3.1 kb)

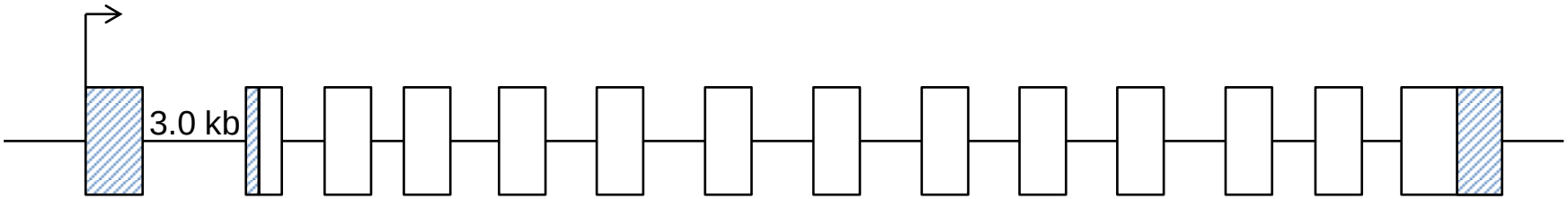

Lamprey *Tp63* isoform (2.8 kb)

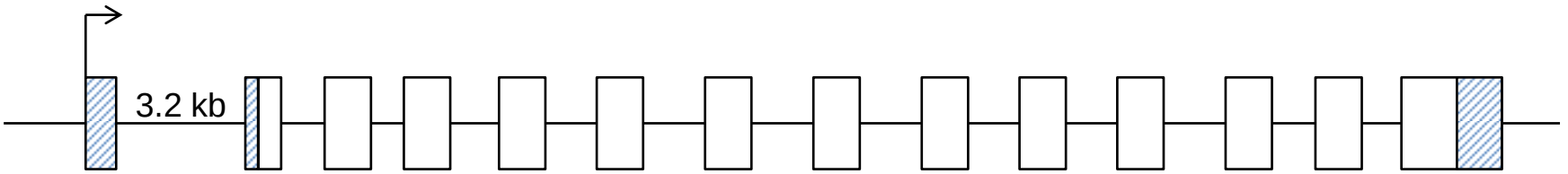

Lamprey *Tp63* isoform (2.6 kb)

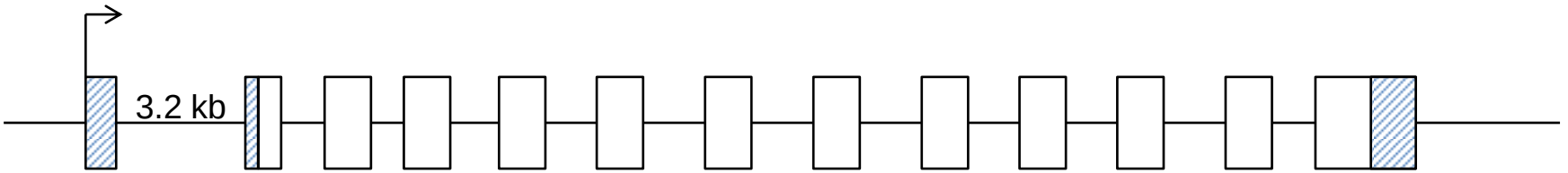

B

Lamprey *Tp73* isoform (2.8 kb)

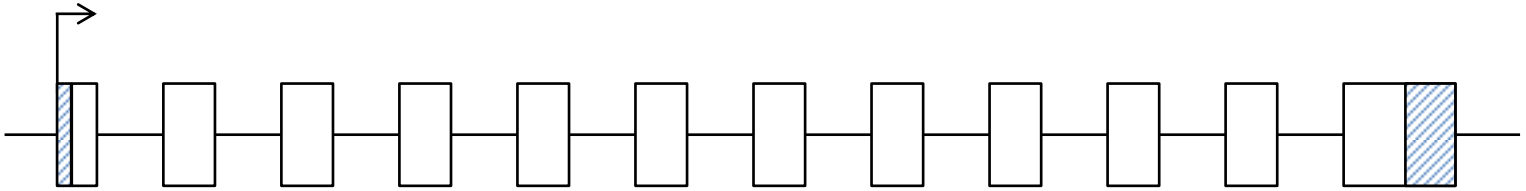

Coffill and Lee *et al.* Fig S7

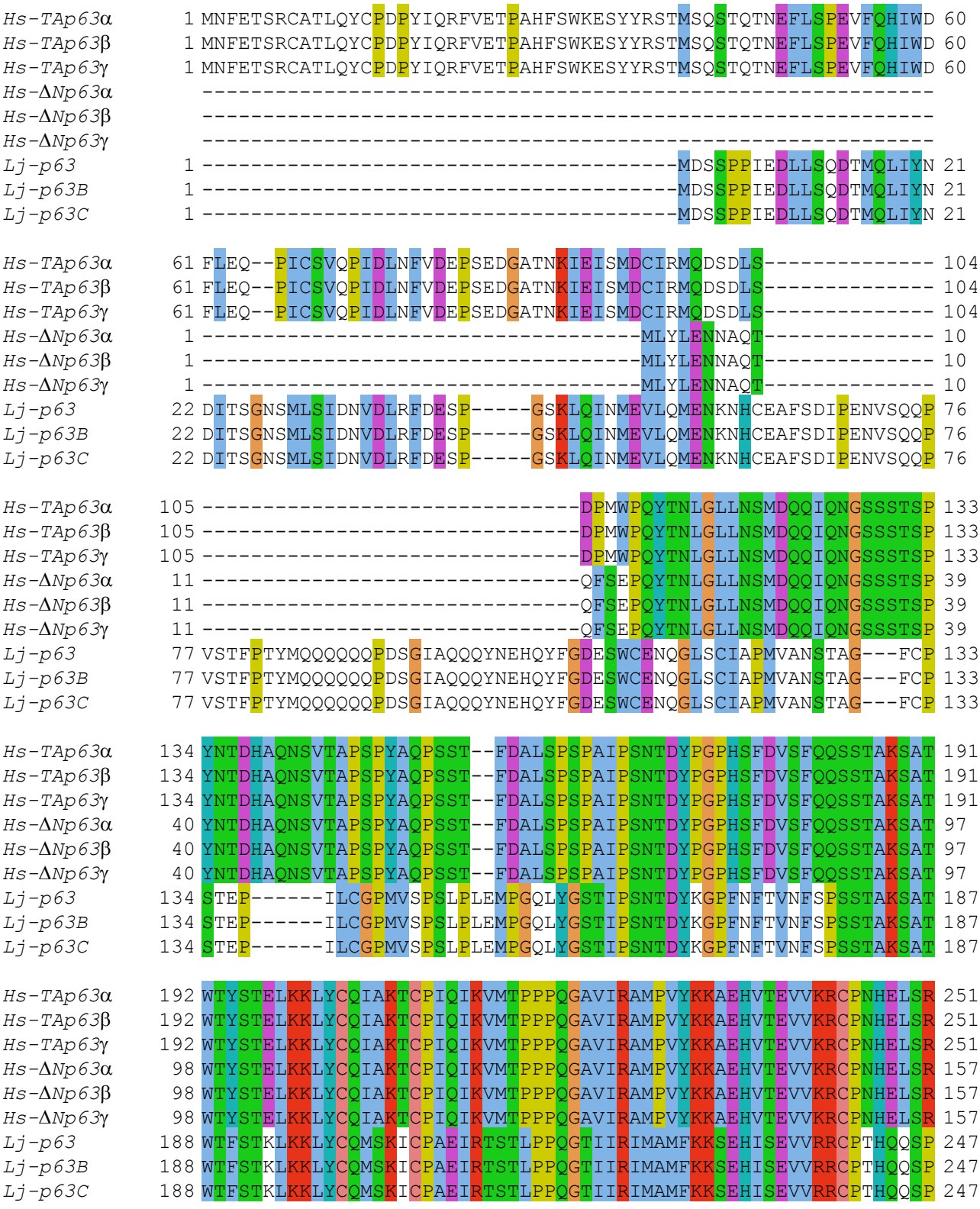

Coffill and Lee *et al.* Fig S8, Panel A

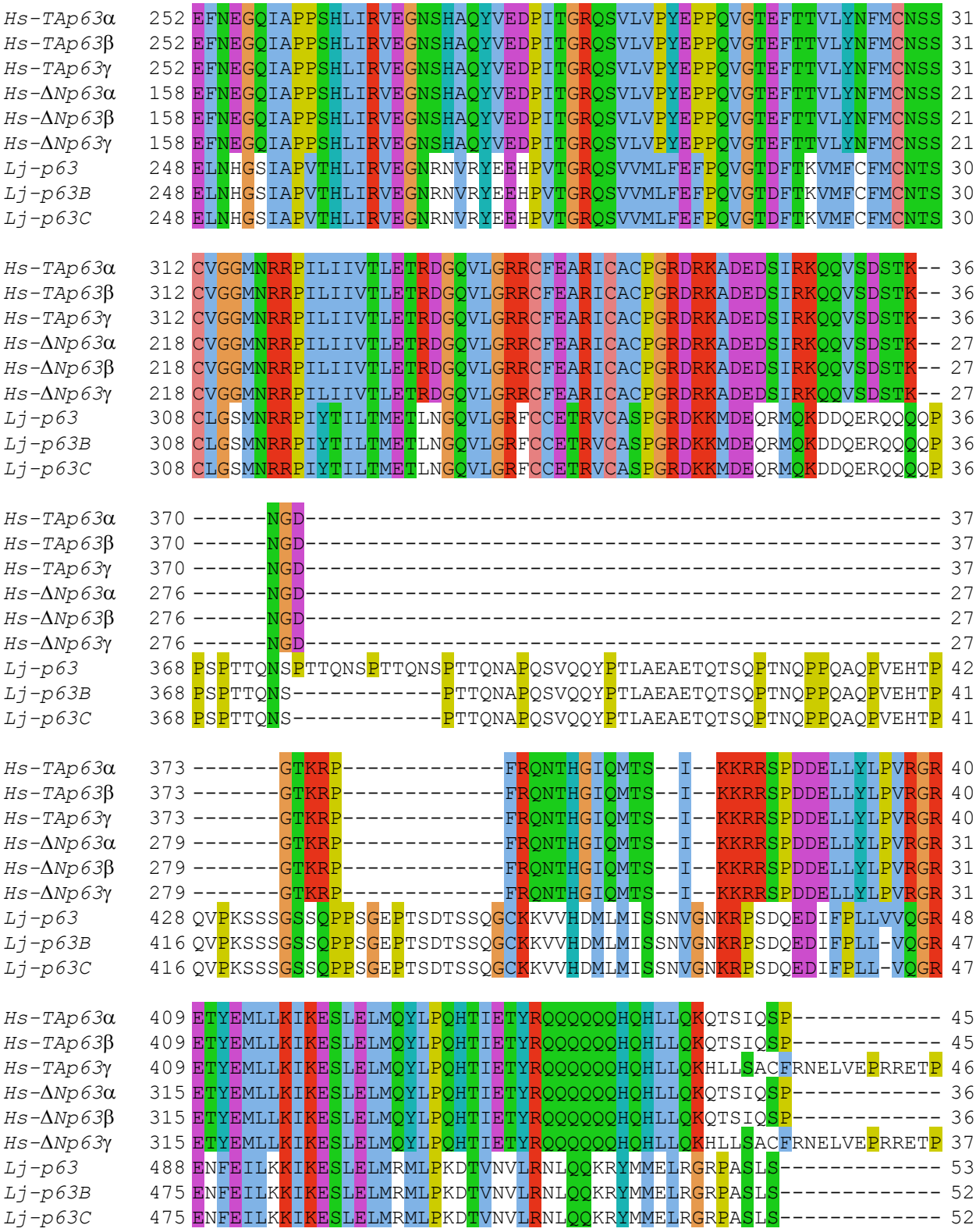

Coffill and Lee *et al.* Fig S8, Panel B

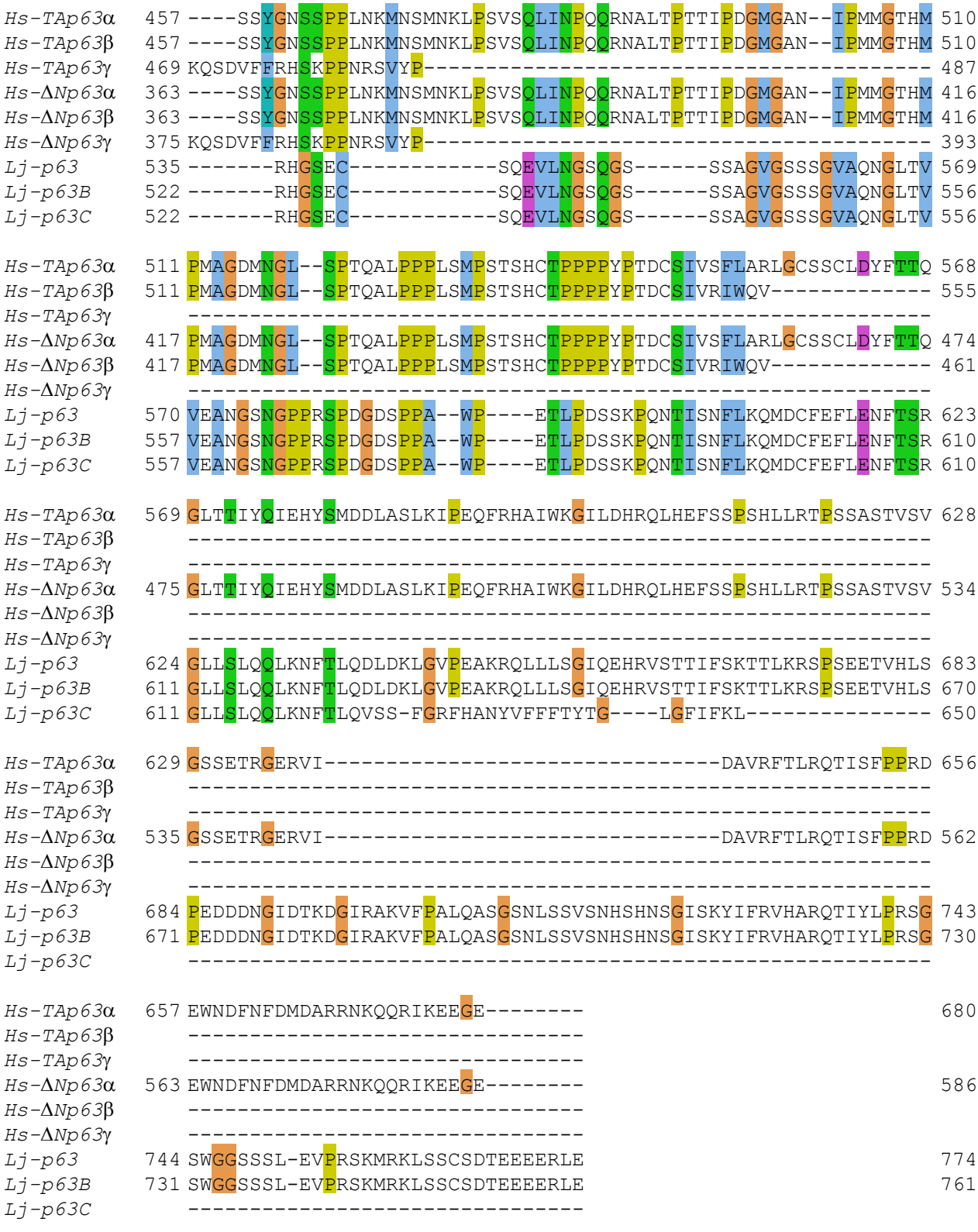

Coffill and Lee *et al.* Fig S8, Panel C

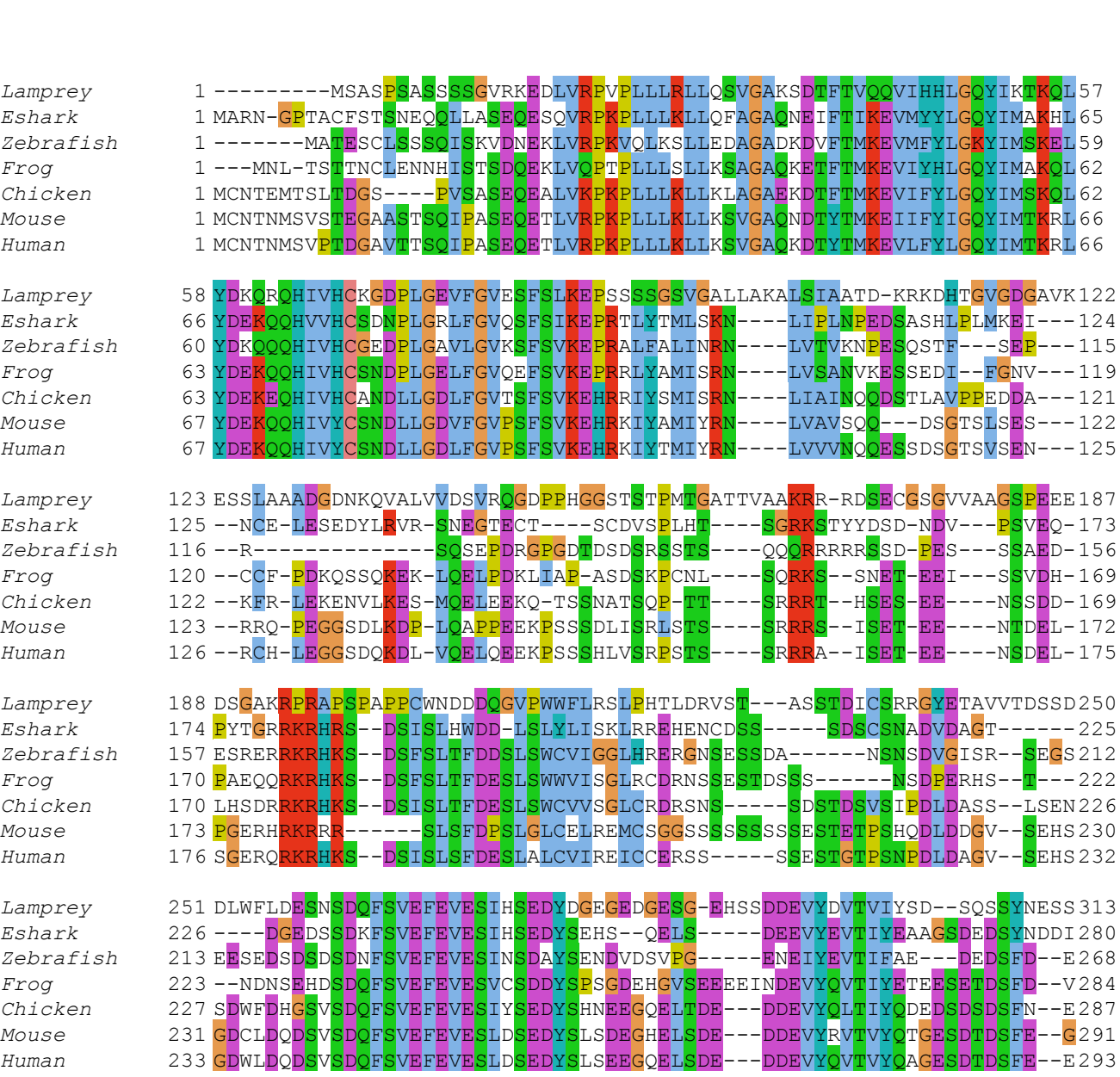

Coffill and Lee *et al.* Fig S9, Panel A

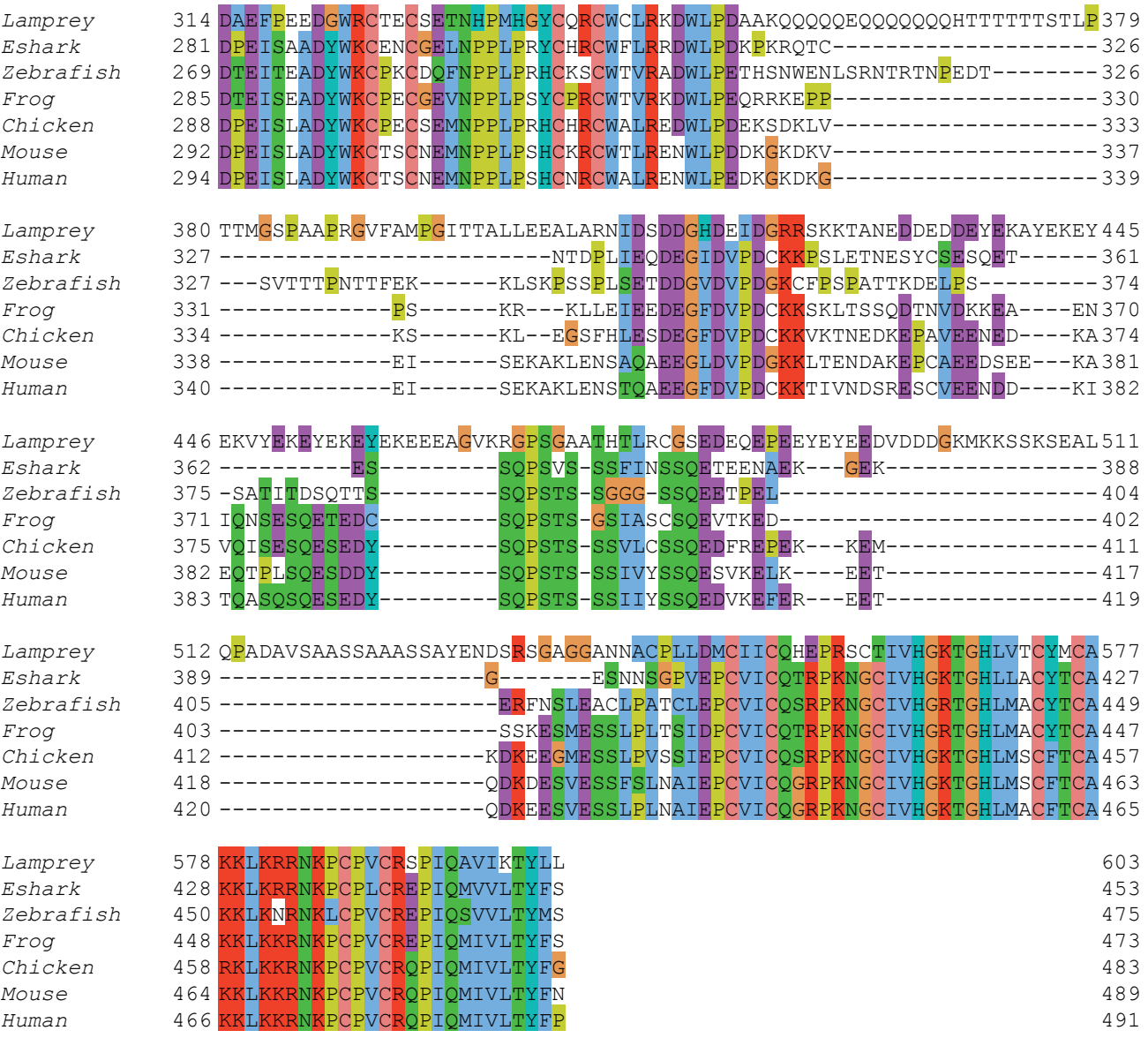

Coffill and Lee *et al.* Fig S9, Panel B

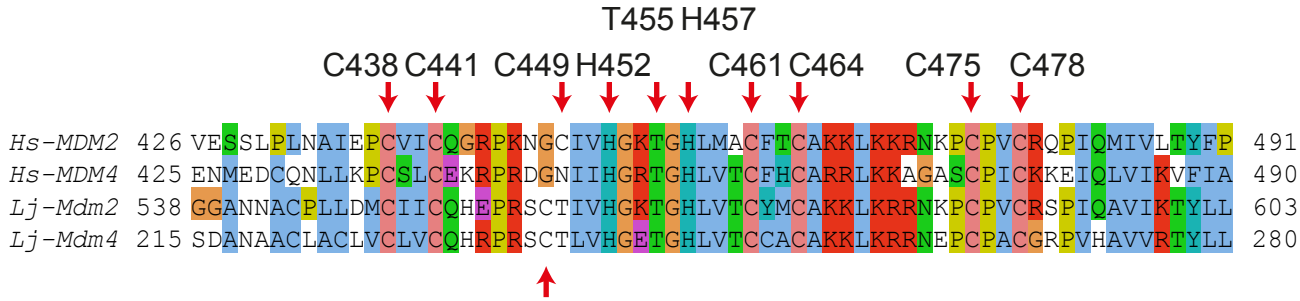

Coffill and Lee *et al.* Fig S10

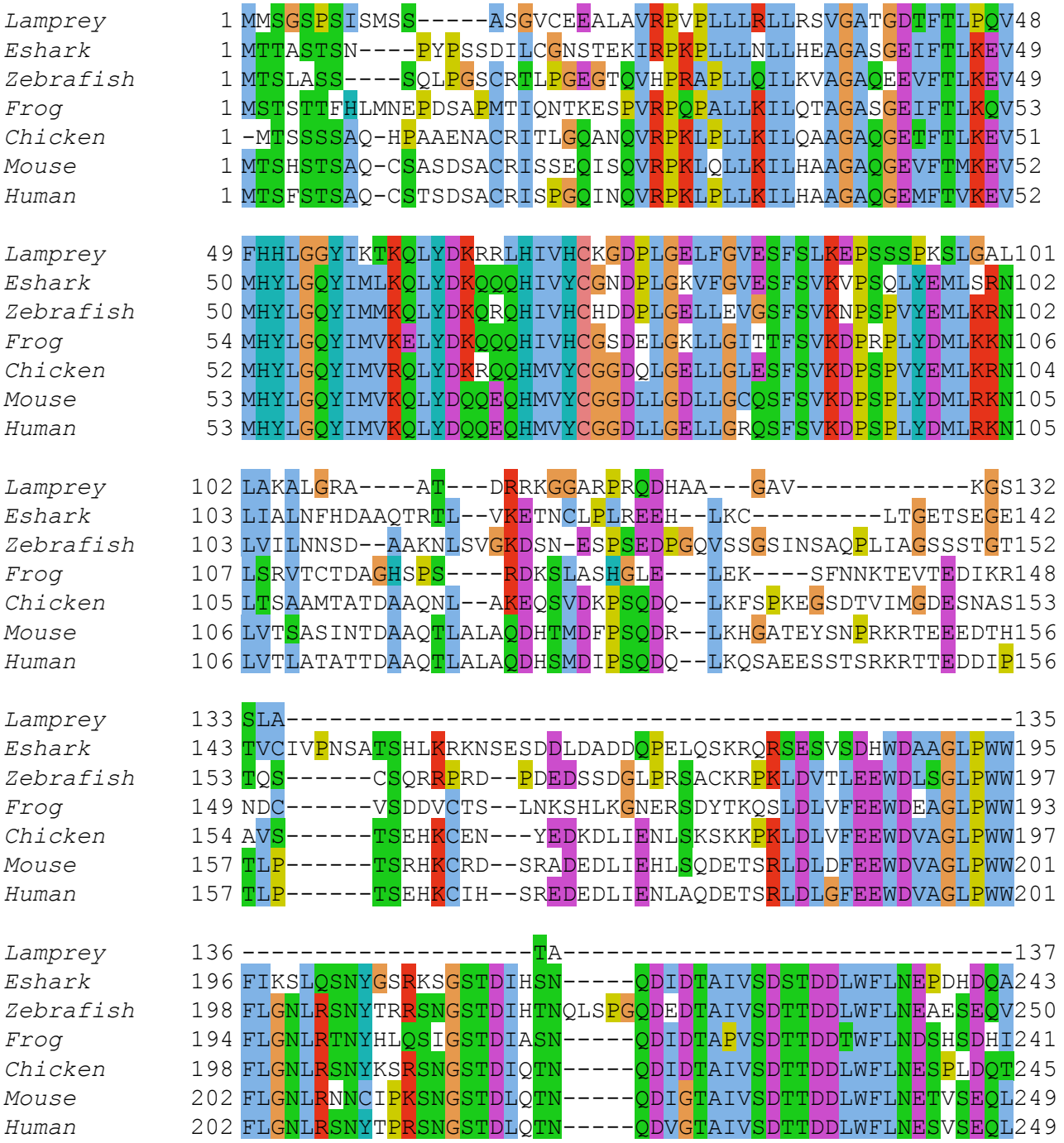

Coffill and Lee *et al.* Fig S11, Panel A

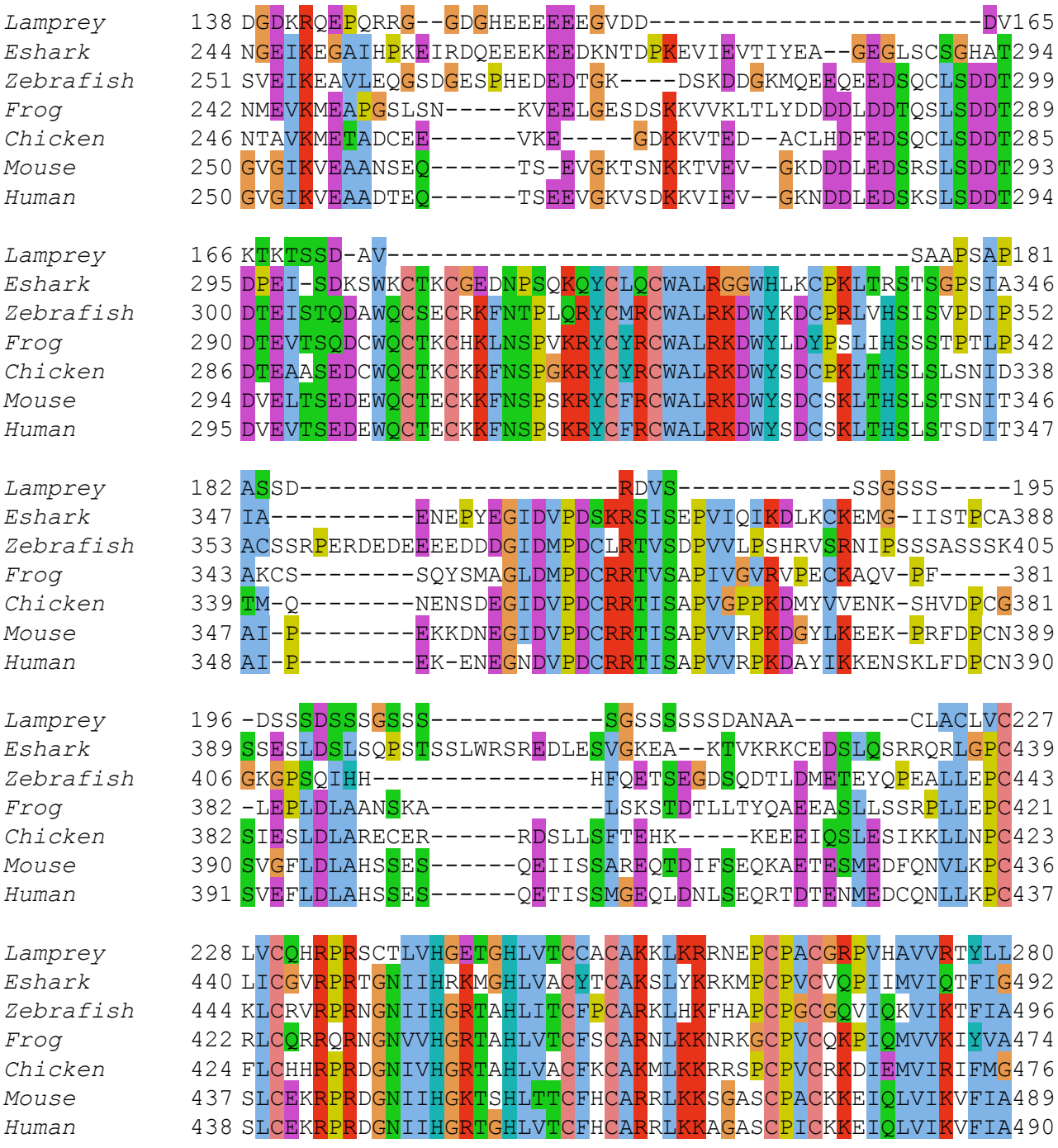

Coffill and Lee *et al.* Fig S11, Panel B

Mdm2 locus

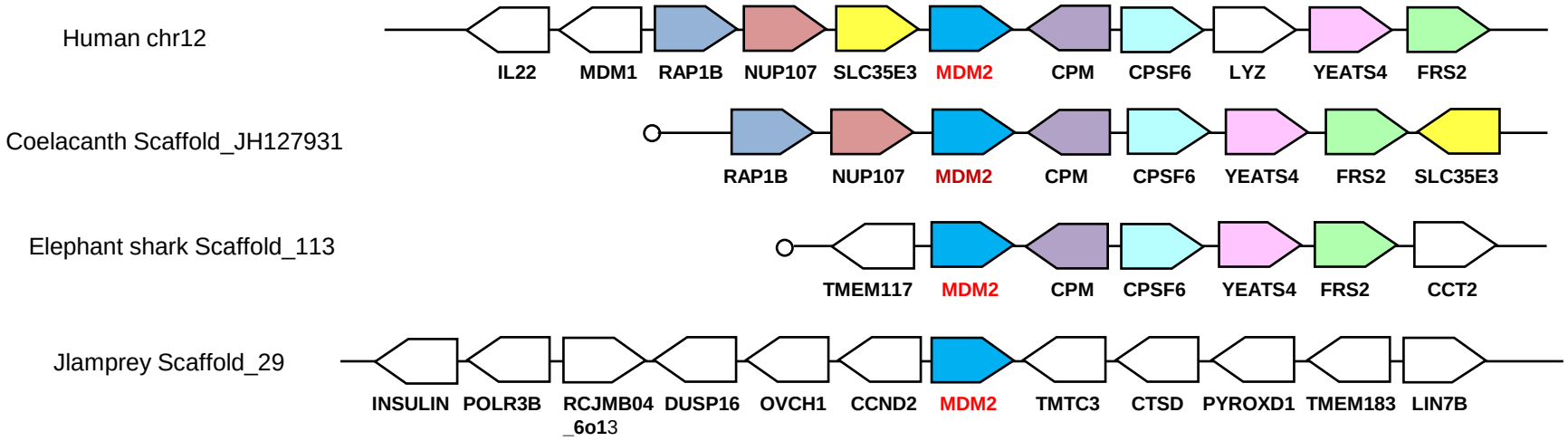

Mdm4 locus

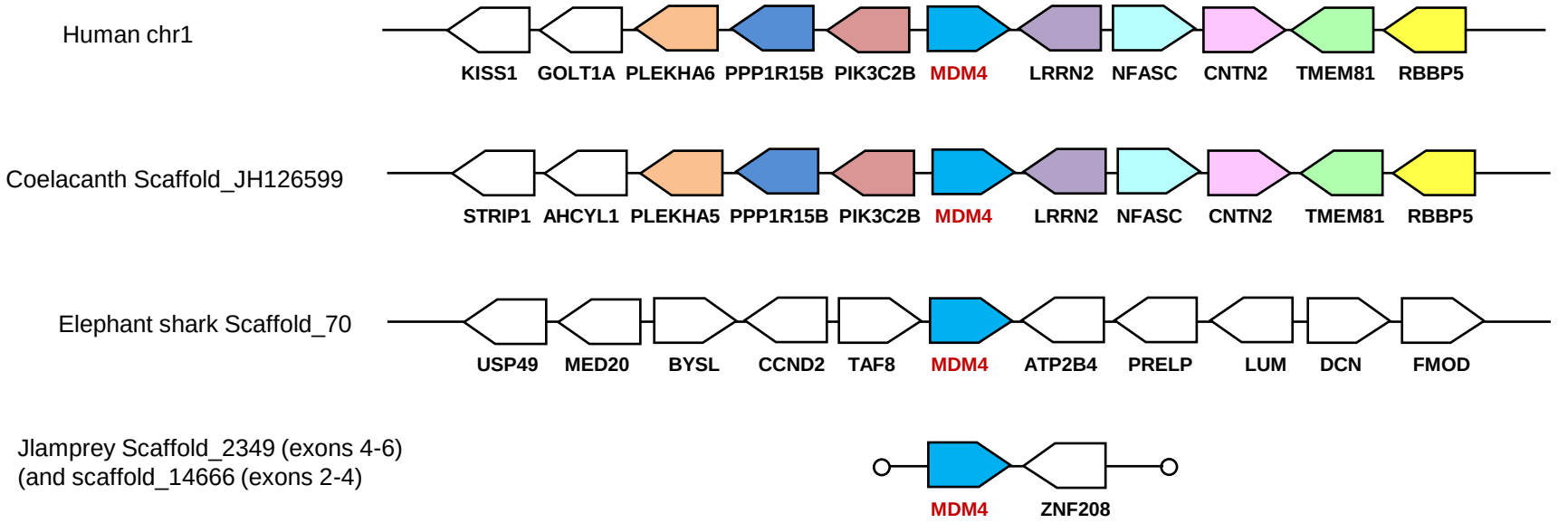

Coffill and Lee *et al.* Fig S12

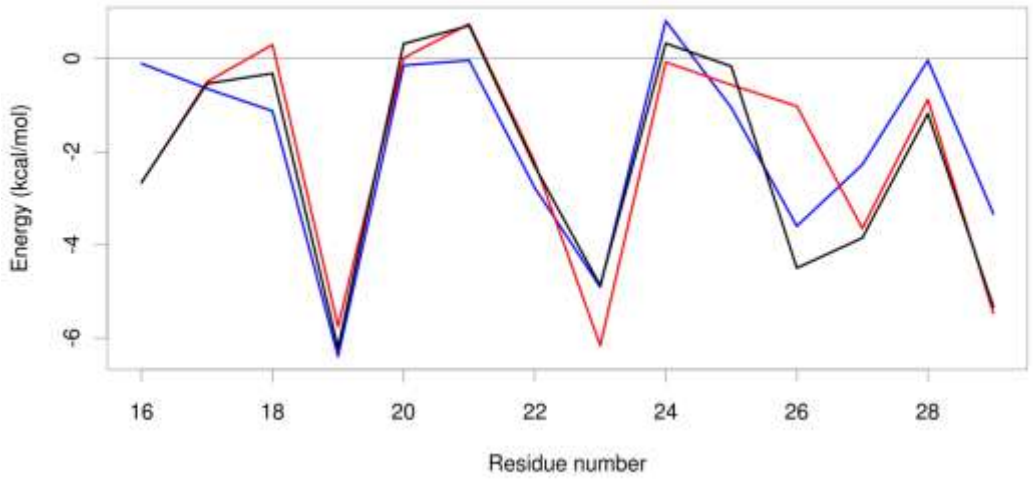

Coffill and Lee *et al.* Fig S13

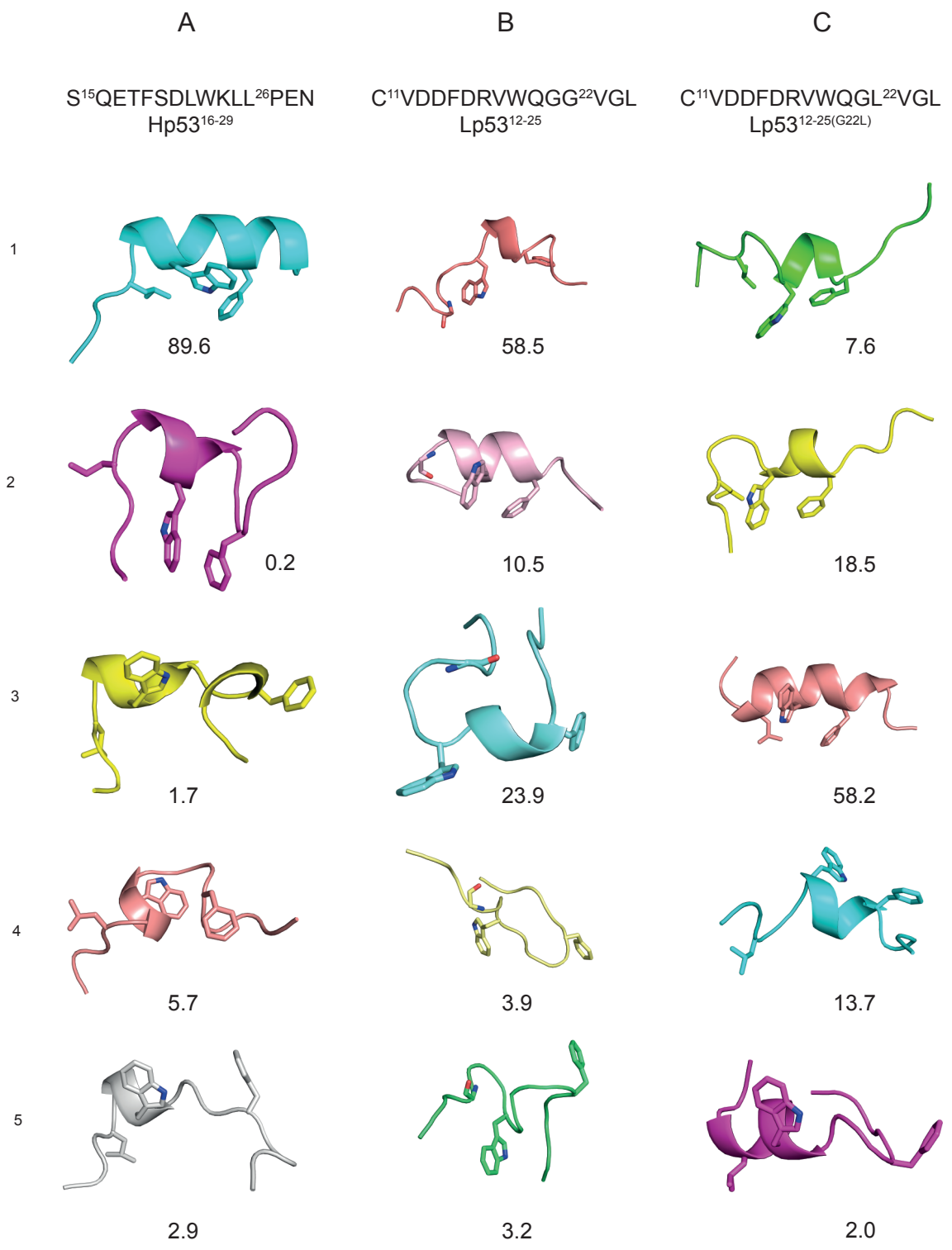

Coffill and Lee *et al.* Fig S14

A

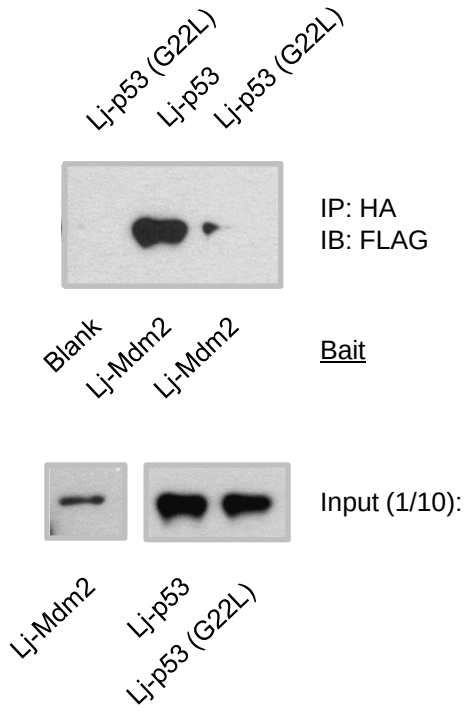

B

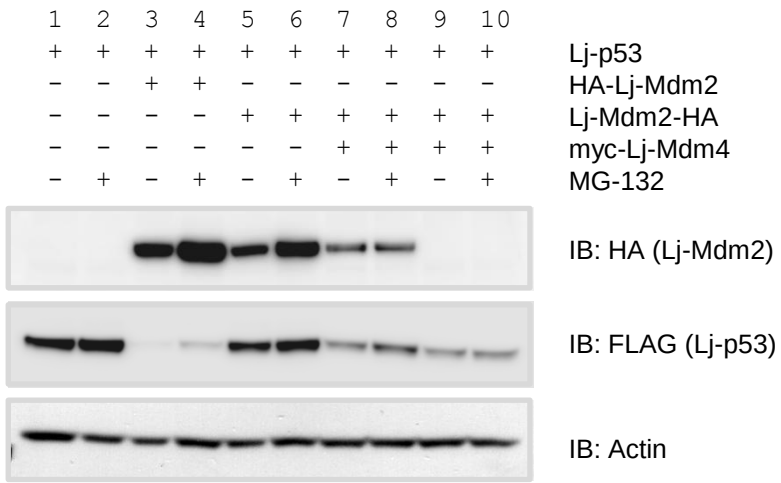

Coffill and Lee *et al.* Fig S15

A

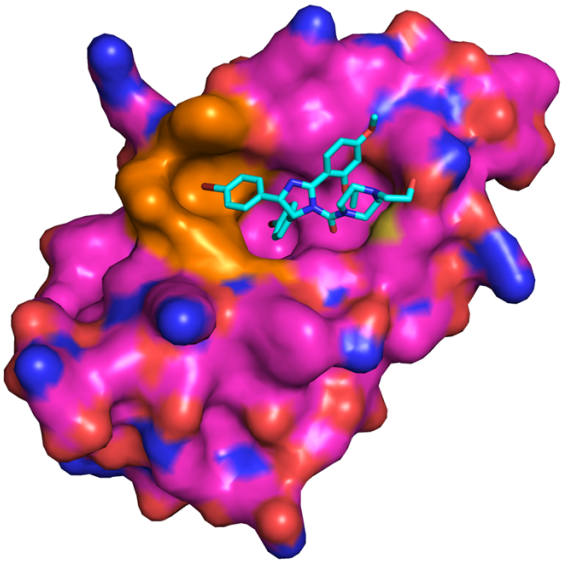

B

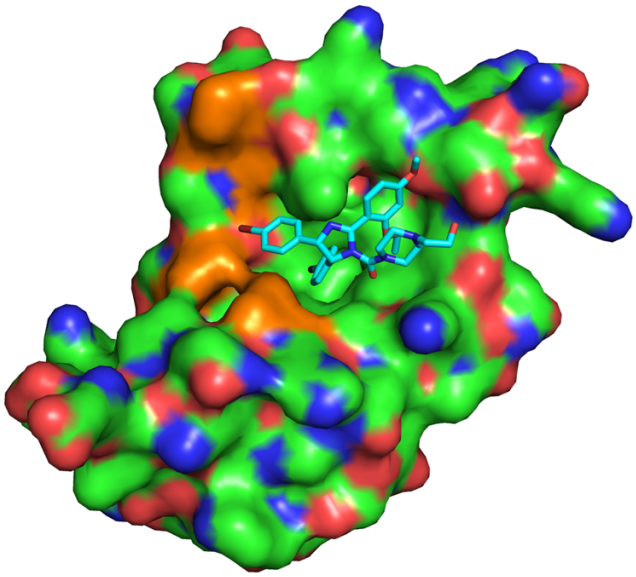

Coffill and Lee *et al.* Fig S16